Local and nonlocal anisotropic transport in reversed shear magnetic fields: Shearless Cantori and nondiffusive transport

Daniel Blazevski
Institute for Mechanical Systems, ETH Zurich, 8092 Zurich, Switzerland

Diego del-Castillo-Negrete
Oak Ridge National Laboratory, Oak Ridge, Tennessee 37831-8071, USA

(Received 15 February 2013; published 10 June 2013)

A study of anisotropic heat transport in reversed shear (nonmonotonic q-profile) magnetic fields is presented. The approach is based on a recently proposed Lagrangian-Green's function method that allows an efficient and accurate integration of the parallel (i.e., along the magnetic field) heat transport equation. The magnetic field lines are described by a nontwist Hamiltonian system, known to exhibit separatrix reconnection and robust shearless ($dq/dr = 0$) transport barriers. The changes in the magnetic field topology due to separatrix reconnection lead to bifurcations in the equilibrium temperature distribution. For perturbations of moderate amplitudes, magnetic chaos is restricted to bands flanking the shearless region. As a result, the temperature flattens in the chaotic bands and develops a very sharp radial gradient at the shearless region. For perturbations with larger amplitude, shearless Cantori (i.e., critical magnetic surfaces located at the minimum of the q profile) give rise to anomalous temperature relaxation involving widely different time scales. The first stage consists of the relatively fast flattening of the radial temperature profile in the chaotic bands with negligible flux across the shearless region that, for practical purposes, on a short time scale acts as an effective transport barrier despite the lack of magnetic flux surfaces. In the long-time scale, heat starts to flow across the shearless region, albeit at a comparatively low rate. The transport of a narrow temperature pulse centered at the reversed shear region exhibits weak self-similar scaling with non-Gaussian scaling functions indicating that transport at this scale cannot be modeled as a diffusive process with a constant diffusivity. Evidence of nonlocal effective radial transport is provided by the existence of regions with nonzero heat flux and zero temperature gradient. Parametric flux-gradient plots exhibit multivalued loops that question the applicability of the Fourier-Fick's prescription even in the presence of a finite pinch velocity.

DOI: 10.1103/PhysRevE.87.063106 PACS number(s): 52.25.Xz, 52.25.Fi, 52.55.Dy

I. INTRODUCTION

Magnetic fields play a critical role in laboratory and astrophysical plasmas. In particular, the use of magnetic fields to confine high temperature plasmas is considered the most promising mechanism for achieving controlled nuclear fusion. Because of this, understanding heat transport in magnetized plasmas is a current open problem in plasma physics research. This problem is particularly challenging because, in general, magnetic fields in three dimensions can have complex structure, including the possibility of being chaotic. Even in two dimensions, where chaos is precluded in the time independent case, the problem can be difficult due to the existence of nontrivial magnetic field topologies involving the reconnection of separatrices linking the hyperbolic points of the field. Beyond the complications brought by the structure of the field lines, the problem is difficult because heat transport in magnetized plasmas is strongly anisotropic; typically, the parallel (i.e., along the field line) heat flux $\mathbf{q}_\parallel$ is many orders of magnitude larger than the perpendicular heat flux $\mathbf{q}_\perp$. To make things worse, in the low collisionality plasmas of interest to controlled fusion, the closure relation of the parallel heat flux typically involves nonlocal operators along the field line, turning the parallel heat transport equation into an integero-differential equation. To circumvent these difficulties, Refs. [1,2] proposed a Lagrangian-Green's (LG) function method that provides an efficient and accurate algorithm for the solution of the heat transport equation in the extreme anisotropic ($\mathbf{q}_\perp = 0$) case. The goal of this paper is to apply the LG method to the case of reversed shear magnetic field configurations.

Reversed shear magnetic field configurations in toroidal devices are characterized by a nonmonotonic poloidal rate of rotation of the magnetic field as function of the minor radius of the torus. These configurations are interesting for at least two reasons. The first one has to do with the experimental observation that these types of configurations typically exhibit very robust transport barriers in toroidal plasma confinement devices [3,4]. The second reason touches a fundamental aspect of the connection between Hamiltonian dynamical systems and magnetic field lines. As it is well known, the symmetry of toroidal confinement devices, along with the divergence condition $\nabla \cdot \mathbf{B} = 0$, imply that the equations describing the field lines orbits are a 1 degree of freedom, possible nonautonomous, Hamiltonian system in which the minor radius and the poloidal angle of the torus correspond to the canonical conjugate variables, and the toroidal angle plays the role of "time." Within this analogy, magnetic field lines that foliate well-defined magnetic flux surfaces correspond to integrable orbits, and chaotic field lines correspond to non-integrable orbits of the Hamiltonian. Of particular theoretical and practical interest is to understand when, why, and how the transition from integrability to chaos takes place. Answering these questions is the goal of Hamiltonian perturbation theory of which the celebrated KAM (Kolmogorov-Arnold-Moser) theorem is one of the main results [5]. However, it turns out that this theorem, as well as other powerful results,

cannot be applied in the case of reversed shear magnetic field configurations because the corresponding Hamiltonian perturbation problem is degenerate at the shearless ($dq/dr = 0$) region where the Hamiltonian violates the twist condition. This brings us back to the second reason why the reversed shear problem is interesting. Namely, the destruction of magnetic flux surfaces in the regions where the magnetic shear vanishes is fundamentally different to what happens in regions where the magnetic shear is finite. This result, which goes beyond the specific plasma physics application, was originally discussed in the more general context of area preserving Hamiltonian nontwist maps in Refs. [6,7] where the resilience of shearless KAM curves was numerically found and the transition to chaos was shown to belong to a universality class different to the one of the nondegenerate Hamiltonian systems. Application of this generic Hamiltonian dynamics result to magnetically confined plasmas include the early works in Refs. [8,9], and the more recent studies reported in Refs. [10,11].

Going beyond these previous studies that limited attention to the dynamics of the magnetic field, here we compute how heat is actually transported when the Hamiltonian describing the field lines is degenerate. In particular, we present the first study on the role of separatrix reconnection and the resilience of shearless barriers (two key signatures of nontwist Hamiltonian systems) on heat transport in reversed shear configurations. As mentioned before, our approach is based on the LG method which allow the uses of general parallel flux closures. Here we consider two cases. The first one is a diffusive closure in which the parallel heat flux is proportional to the local temperature gradient along the field line. The second case corresponds to a nonlocal closure in which the heat flux depends on the global temperature distribution along the whole field line. This regimen is of importance in the study of high temperature, low collisionality plasmas [12]. The mathematical model adopted here to study this case is based on fractional diffusion operators. These operators provide a unifying framework to describe nondiffusive transport in plasmas when the standard Fourier-Fick's law fails to apply [13].

The specific problems that we address in the present paper are: (i) The role of separatrix reconnection on heat transport; (ii) the role of shearless Cantori on the relaxation of the radial temperature profile; and (iii) nonlocal effective radial transport. Separatrix reconnection is an ubiquitous global bifurcation in nontwist Hamiltonian systems, see for example [6,14–16] and references therein. Here we study how the resulting changes in the magnetic field topology lead to bifurcations in the steady state radial temperature profile. At the threshold of the transition to chaos, magnetic field lines trace Cantor-like fractal sets in the Poincare section. Following the dynamical systems terminology [17], we refer to these structures as "Cantori." Our goal here is to study the role of these partial barriers on the equilibration of the temperature across the reversed shear region. Finally, regarding nonlocal effective transport, we provide numerical evidence of the violation of the Fourier-Fick's prescription for the radial transport of temperature.

The rest of this article is organized as follows. The next section presents a review of the Lagrangian Green's function (LG) method. The reversed shear magnetic field model is presented in Sec. III along with a discussion of the connection with nontwist Hamiltonian systems. The core of the numerical results are presented in Sec. IV. Section V contains the conclusions.

II. LG METHOD FOR DIFFUSIVE AND NONLOCAL FRACTIONAL PARALLEL TRANSPORT

In this section we review the method to compute heat transport along magnetic field lines developed in Refs. [1,2]. The starting point is the heat transport equation

$$\partial_t T = -\nabla \cdot \mathbf{q} + S, \tag{1}$$

where $\mathbf{q}$ is the heat flux and S is a source. The flux is decomposed into a parallel (along the magnetic field) and a perpendicular component $\mathbf{q} = q_\parallel \hat{\mathbf{b}} + \mathbf{q}_\perp$, where $\hat{\mathbf{b}} = \mathbf{B}/|B|$ is the unit magnetic field vector. Motivated by the strong anisotropy typically encountered in magnetized plasmas (e.g., $\chi_\parallel/\chi_\perp \sim 10^{10}$ in fusion plasmas, where $\chi_\parallel$ and $\chi_\perp$ denote the parallel and perpendicular conductives) we limit attention to parallel heat transport in the extreme anisotropic regime, i.e., we assume $\mathbf{q}_\perp = 0$. To close the system, Eq. (1) needs to be complemented with a relationship between the parallel heat flux and the temperature,

$$q_\parallel = \chi_\parallel \mathcal{Q}[T], \tag{2}$$

where $\mathcal{Q}$ denotes a general differential or integro-differential, possibly nonlinear, operator. Substituting Eq. (2) into Eq. (1) gives

$$\partial_t T + \chi_\parallel (\nabla \cdot \hat{\mathbf{b}}) \mathcal{Q} = -\chi_\parallel \partial_s \mathcal{Q} + S, \tag{3}$$

where $\nabla \cdot \hat{\mathbf{b}} = -(\partial_s B)/B$, and $\partial_s = \hat{\mathbf{b}} \cdot \nabla$ denotes the directional derivative along the magnetic field line with s the arc-length parameter. In deriving Eq. (3), we have assumed that the parallel diffusivity is constant along the field line, i.e., $\partial_s \chi_\parallel = 0$. Throughout this paper we neglect the second term on the left-hand side of Eq. (3). That is, we assume $|(\partial_s B)/B| \ll |(\partial_s \mathcal{Q})/\mathcal{Q}|$, and write the parallel transport equation as

$$\partial_t T = -\chi_\parallel \partial_s \mathcal{Q} + S. \tag{4}$$

This approximation (known as toroidal ordering in fusion plasmas) is commonly used in the study of magnetically confined plasmas in the presence of a strong guiding field. In particular, it is a good approximation in cylindrical geometry, $\mathbf{B} = \mathbf{B}_0 + \epsilon \mathbf{B}_1$, where $\mathbf{B}_0$ is a helical field for which $\partial_s B_0 = 0$, and $\epsilon B_1 \ll B_0$. In the calculations presented here, $\epsilon \sim 10^{-4}$ and $|(\partial_s B)/B| \sim 10^{-3}$.

The specific form of the operator $\mathcal{Q}$ depends on the physics of the closure relating the heat flux and the temperature. For high collisionality plasmas, parallel transport is typically dominated by diffusion and a Fourier-Fick's type local flux-gradient relation of the form

$$\mathcal{Q}[T] = -\partial_s T \tag{5}$$

is assumed. Substituting Eq. (5) into Eq. (1), leads to the standard diffusion equation

$$\partial_t T = \chi_\parallel \partial_s^2 T + S, \tag{6}$$

for collisional transport along magnetic field lines.

However, for low collisionality plasmas, the parallel flux closure is in general nonlocal [12]. That is, the heat flux at a point depends not only on the local properties of the temperature (i.e., its gradient) but on the temperature distribution along the whole magnetic field line. As a tractable model to study nonlocal heat transport along magnetic field lines, following [13], we consider the fractional diffusion equation

$$\partial_t T = \chi_\parallel \partial^\alpha_{|s|} T + S, \tag{7}$$

where $\partial^\alpha_{|s|}$ denotes the symmetric fractional derivative of order α along the field line, defined in Fourier space as

$$\widehat{\partial^\alpha_{|s|} T} = -|k|^\alpha \hat{T}, \tag{8}$$

where $\hat{T} = \int_{-\infty}^{\infty} e^{iks} T(s) ds$ denotes the Fourier transform. For $\alpha = 2$, $\partial^\alpha_{|s|} T$ formally reduces to the diffusion operator $\partial^2_x T$. For $1 \leqslant \alpha < 2$, the nonlocal flux closure corresponding to the fractional diffusion model in Eq. (7) is

$$\mathcal{Q}[T] = -\frac{\lambda_\alpha}{\pi} \int_0^\infty \frac{T(s+z) - T(s-z)}{z^\alpha} dz, \tag{9}$$

with $\lambda_\alpha = -\pi(\alpha-1)/[2\Gamma(2-\alpha)\cos(\alpha\pi/2)]$, where Γ denotes the Gamma function. For $\alpha = 1$, the fractional flux closure in Eq. (9) reduces to the free streaming case [12].

Figure 1 illustrates the LG method proposed in Refs. [1,2] for the solution of the anisotropic heat transport equation for a time-independent magnetic field in the limit $\mathbf{q}_\perp = 0$. Given an initial temperature distribution $T_0(\mathbf{r}) = T(\mathbf{r}, t=0)$, and a source $S(\mathbf{r},t)$, the temperature at a given point in space $\mathbf{r}_0$, at a time t, is obtained by summing all the contributions of the initial condition and the source along the magnetic field line path:

$$T(\mathbf{r}_0,t) = \int_{-\infty}^{\infty} T_0[\mathbf{r}(s')] \mathcal{G}_\alpha(s',t) ds' + \int_0^t dt' \int_{-\infty}^{\infty} ds' S[\mathbf{r}(s'),t'] \mathcal{G}_\alpha(s', t-t'), \tag{10}$$

where $\mathcal{G}_\alpha$ is the Green's function of the parallel transport equation, and $\mathbf{r}(s)$ denotes the magnetic field line trajectory obtained from the solution of the initial value problem

$$\frac{d\mathbf{r}}{ds} = \hat{\mathbf{b}}, \quad \mathbf{r}(0) = \mathbf{r}_0, \tag{11}$$

where s is the arc length.

As it is well known, in an unbounded domain, for $\alpha = 2$, $\mathcal{G}_2$ is given by the Green's function of the diffusion Eq. (6),

$$\mathcal{G}_2(s,t) = \frac{1}{\sqrt{2\pi}} (\chi_\parallel t)^{-1/2} \exp\left(-\frac{s^2}{4\chi_\parallel t}\right), \tag{12}$$

and for general α, $\mathcal{G}_\alpha$ is given by the Green's function of the fractional diffusion Eq. (7),

$$\mathcal{G}_\alpha = \frac{1}{(\chi_\parallel t)^{\frac{1}{\alpha}}} L_\alpha \left[\frac{s}{(\chi_\parallel t)^{\frac{1}{\alpha}}}\right], \tag{13}$$

where

$$L_\alpha(\eta) = \frac{1}{2\pi} \int_{-\infty}^{\infty} e^{-|k|^\alpha - i\eta k} dk \tag{14}$$

is the symmetric α-stable Levy distribution. The case $\alpha = 1$, which corresponds to the commonly used nonlocal free streaming closure, has the analytically simple expression

$$\mathcal{G}_1(s,t) = \frac{(\chi_\parallel t)^{-1}}{\pi} \frac{1}{1 + (s/\chi_\parallel t)^2}. \tag{15}$$

The numerical implementation of the LG method requires three elements: an ODE integrator for solving the field line trajectories in Eq. (11), an interpolation procedure of the function $T_0(\mathbf{r})$ on the field line, and a numerical quadrature to evaluate the Green's function integral in Eq. (10). These elements are relatively straightforward to implement numerically, making the LG algorithm a versatile, efficient, and accurate method for the computation of heat transport in magnetized plasmas. By construction, the method preserves the positivity of the temperature evolution and avoids completely the pollution issues encountered in grid-based algorithms. Also, because of the parallel nature of the Lagrangian calculation, the formulation naturally leads to a massively parallel implementation. In particular, the computation of T at $\mathbf{r}_0$ at time t does not require the computation of T in the neighborhood of $\mathbf{r}_0$, as it is the case in finite different methods, or the computation of T at previous times. Further details on the method and the numerical implementation can be found in Refs. [1,2].

As mentioned before, throughout this paper we limit attention to purely parallel transport. However, as discussed in Ref. [18], the LG method can be extended to include finite perpendicular transport, i.e., $\chi_\perp \neq 0$. The key idea is to formally include the perpendicular transport channel as

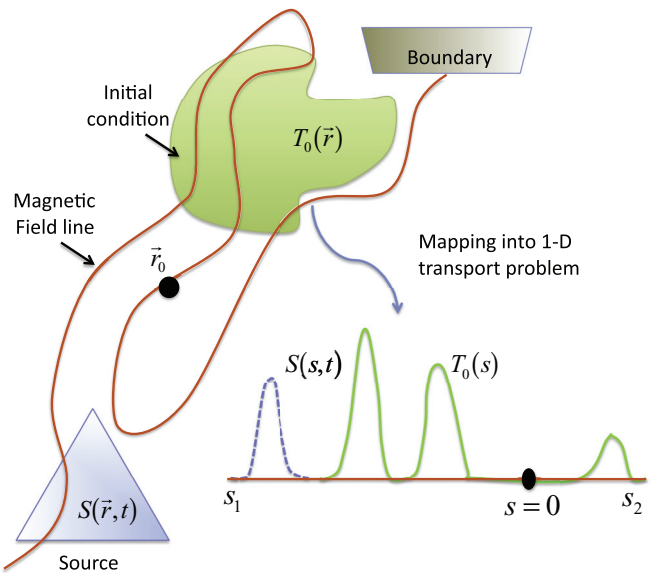

FIG. 1. (Color online) Schematics of Lagrangian-Green's function (LG) method [1,2]. When $\mathbf{q}_\perp = 0$, the temperature at point $\mathbf{r}_0$, at time t, depends only on the heat transported along the unique magnetic field line passing through $\mathbf{r}_0$. The problem then reduces to the solution of a 1D transport problem with initial condition $T_0(\mathbf{r}(s))$ and source $S(\mathbf{r}(s),t)$, where $\mathbf{r} = \mathbf{r}(s)$ is the magnetic field line trajectory parametrized by the arc length, with $\mathbf{r}(s=0) = \mathbf{r}_0$. If $\mathcal{G}_\alpha$ is the Green's function of the transport operator, $T(\mathbf{r}_0,t)$ is computed directly by evaluating the integrals in Eq. (10).

part of an effective source $S^* = S + \chi_\perp \nabla_\perp T$ in Eq. (7), and use the formal LG solution in Eq. (10) to transform the heat transport equation into an integro-differential equation. The numerical solution of the integro-differential equation is based on a semi-Lagrangian operator-splitting algorithm consisting of two steps. The first step is the Eulerian solution of the perpendicular transport equation, and the second step is the solution of the parallel transport equation with source using the LG method.

III. REVERSED SHEAR MAGNETIC FIELD MODEL AND NONTWIST HAMILTONIAN SYSTEMS

We assume a periodic straight cylindrical domain with period $L = 2\pi R$, and use cylindrical coordinates (r,θ,z). The magnetic field is given by

$$\mathbf{B}(r,\theta,z) = \mathbf{B}_0(r) + \mathbf{B}_1(r,\theta,z), \tag{16}$$

where

$$\mathbf{B}_0 = \left[\frac{r}{R}\frac{B_0}{q(r)}\right]\hat{\mathbf{e}}_\theta + B_0\hat{\mathbf{e}}_z \tag{17}$$

is a helical field with B_0 constant, and $\mathbf{B}_1(r,\theta,z)$ is a perturbation. The function $q(r)$ in Eq. (17), known as the safety factor, determines the shear of the helical magnetic field, i.e., the dependence of the azimuthal rotation of the field as function of the radius. In the present paper we assume

$$q(r) = q_0\left[1 + \lambda^2\left(r - \frac{1}{\sqrt{2}}\right)^2\right], \tag{18}$$

which, as shown in Fig. 2, is nonmonotonic in r and has a minimum at $r = r_{sl} = \frac{1}{\sqrt{2}}$. This implies a reversal of the magnetic field shear which is positive for $r < r_{sl}$, negative for $r > r_{sl}$, and vanishes at the shearless point $r = r_{sl}$. For the value of the model parameters, we take $R = 5$, $B_0 = 1$, $q_0 = 0.64$, and $\lambda = 3.0$. The functional form of the q profile and the parameter values were chosen to have the reversed shear region in the middle of the computational domain (in the $R^2\psi$ variables) and to guarantee that modes with $m/n < 1$ exhibit two resonances. We assume that the perturbation $\mathbf{B}_1$ has no z component and write it as

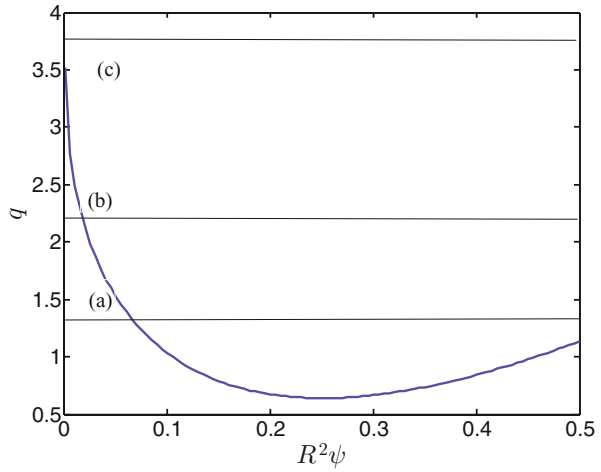

FIG. 2. (Color online) q profile in Eq. (18) as a function of radial flux coordinate $R^2\psi$ in the reversed shear magnetic field configuration used in the calculations. For a given m/n, resonances are located where $q(R^2\psi) = m/n$. For the values corresponding to (a), (b), and (c) in the plot, there are two, one, and zero resonances, respectively.

$$\mathbf{B}_1 = \nabla \times [A_z(r,\theta,z)\hat{\mathbf{e}}_z], \tag{19}$$

where the magnetic potential A_z has the form

$$A_z(r,\theta,z) = \sum_{m,n} A_{mn}(r)\cos\left(m\theta - \frac{nz}{R} + \zeta_{mn}\right). \tag{20}$$

To explain the connection of the reversed shear model with nontwist Hamiltonian systems, recall that the magnetic field line trajectories parametrized by λ, $\lambda \to \mathbf{r}(\lambda)$, are determined by the solution of the equations $dr/d\lambda = B_r$, $rd\theta/d\lambda = B_\theta$, $dz/d\lambda = B_z$. For the magnetic field model in Eqs. (17)–(20) this implies

$$\frac{dr}{d\lambda} = \frac{1}{r}\frac{\partial A_z}{\partial\theta}, \quad \frac{d\theta}{d\lambda} = \frac{B_0}{Rq(r)} - \frac{1}{r}\frac{\partial A_z}{\partial r}, \quad \frac{dz}{d\lambda} = B_0. \tag{21}$$

Since B_0 is assumed constant, the dynamics in the z direction is trivial, and $z = B_0\lambda$ can be used to parametrize the field line orbits. Doing this and defining

$$\psi = \frac{r^2}{2R^2}, \quad H(\psi,\theta,z) = H_0(\psi) + H_1(\psi,\theta,z), \tag{22}$$

where

$$H_0 = \frac{1}{R}\int\frac{d\psi}{q(\psi)}, \quad H_1 = -\frac{1}{B_0R^2}A_z(\psi,\theta,z), \tag{23}$$

the equations for the magnetic field lines for the nontrivial r and θ components can be written as the canonical Hamiltonian system

$$\frac{d\theta}{dz} = \frac{\partial H}{\partial\psi}, \quad \frac{d\psi}{dz} = -\frac{\partial H}{\partial\theta}. \tag{24}$$

In the absence of a perturbation, $\mathbf{B}_1 = H_1 = 0$, Eqs. (24) are trivially integrable and

$$\theta = \theta_0 + \Omega(\psi_0)\frac{z}{R}, \quad \psi = \psi_0, \tag{25}$$

where (θ_0,ψ_0) denotes the initial condition and

$$\Omega(\psi) = \frac{\partial^2 H_0}{\partial\psi^2} = \frac{1}{q(\psi)} \tag{26}$$

is the unperturbed rotation frequency. The study of the fate of these integrable orbits in the presence of the perturbation H_1 is the subject matter of Hamiltonian perturbation theory. As it is well known, whereas some of the integrable orbits are just slightly deformed when $H_1 \neq 0$, others are fundamentally altered and can become chaotic. Determining how and when the transition from integrability to chaotic behavior happens is a highly nontrivial dynamical systems problem of key interest to controlled fusion because of the favorable confinement properties of nonchaotic magnetic fields. However, what makes this problem particularly challenging in the case studied in the present paper is that the nonmonotonicity of the q profile in Eq. (18) implies that there is a value of $\psi = \psi_{sl}$ for which the shear of the rotation frequency vanishes, i.e., $d\Omega/d\psi = 0$ at $\psi = \psi_{sl}$. Because of this, the *nondegeneracy*

condition

$$\left.\frac{\partial^2 H_0}{\partial \psi^2}\right|_{\psi_{sl}} \neq 0, \tag{27}$$

that is a cornerstone in the justification of key dynamical systems results including the celebrated standard KAM (Kolmogorov-Arnol-Moser) theorem [5], does not hold. As originally discussed in Refs. [6,7], one of the main consequences of the breakdown of the nondegeneracy condition is the remarkable resilience of integrable orbits in shearless regions which implies that transport barriers typically exist in these regions. In the context of magnetically confined plasmas this naturally leads to the conclusion that robust magnetic flux surfaces typically form in reversed shear magnetic field configurations as pointed out in Refs. [6,8] and subsequent papers including Refs. [9–11]. In addition to the robustness of shearless transport barriers, nontwist Hamiltonian systems [i.e., systems that do not satisfy Eq. (27)] exhibit nontrivial changes in the phase space topology due to separatrix reconnection [6,14–16]. As mentioned in the Introduction, one of the main goals of the present paper is to explore the role on parallel transport of these two signatures of reversed shear configurations, namely, the robustness of transport barriers and separatrix reconnection.

The magnetic field perturbation in Eq. (20) is chosen so that the function $A_{mn}(\psi)$ is peaked at the resonance(s) for each (m,n). We recall that a resonance r^* is defined by the condition $q(r^*) = m/n$. Due to the nonmonotonicity of the q profile, as Fig. 2 indicates, it is possible to have two, one, or no resonances depending on the value of m/n. In the case when there are no resonances for (m,n), $A_{mn} = 0$. When there are two resonances for a given (m,n), we take

$$A_{mn}(r) = \epsilon a(r)(A_{mn,1} + A_{mn,2}), \tag{28}$$

where ϵ is a small free parameter and

$$A_{mn,i} = C_{mn,i} r^m \exp\left[-\left(\frac{r - r_{0i}}{\sqrt{2}\sigma}\right)^2\right], \tag{29}$$

for $i = 1,2$. The width σ controls the overlap of $A_{mn,1}$ and $A_{mn,2}$, which increases near the minimum of the q profile, where the resonances are close to each other. For the modes used in the numerical simulations presented here, it was observed that $\sigma = 0.05$ is sufficient to guarantee negligible overlap. To guarantee the vanishing of the perturbation at the boundary, and the existence of good flux surfaces there, we assume $a(r) = \{1 - \tanh[(r-1)/0.05]\}/2$, which decays exponentially fast near $r = 1$. The prefactor r^m is introduced to ensure the regularity of the perturbation at $r = 0$. The constants

$$\begin{aligned} r_{0i} &= r_{i*} - \frac{m\sigma^2}{r_{i*}}, \\ C_{mn,i} &= \left(\frac{1}{r_{*i}}\right)^m \exp\left[\left(\frac{r_{i*} - r_{0i}}{\sqrt{2}\sigma}\right)\right], \end{aligned} \tag{30}$$

for $i = 1,2$, are chosen to satisfy the conditions

$$\frac{dA_{mn,i}}{dr}(r_{i*}) = 0, \quad A_{mn,i}(r_{i*}) = 1, \tag{31}$$

that guarantee that $A_{mn,i}$ has a maximum with unit amplitude at the location of the resonance $r = r_{i*}$. Finally, in the case when there is only one resonance for the mode (m,n),

$$A_{mn}(r) = \epsilon a(r) A_{mn,1}, \tag{32}$$

where $A_{mn,1}$ is given in Eq. (29) with $i = 1$.

IV. HEAT TRANSPORT IN INTEGRABLE, WEAKLY CHAOTIC, AND FULLY CHAOTIC REVERSED SHEAR MAGNETIC FIELDS

In this section we apply the Lagrangian-Green's function method to compute parallel transport in the reversed shear magnetic field model in the integrable, weakly chaotic, and fully chaotic regimes.

A. Separatrix reconnection and heat transport in integrable fields

For single-mode perturbations the magnetic field is fully integrable. However, the magnetic field topology can exhibit bifurcations due to separatrix reconnection, and in this subsection we study the effect of these bifurcations on transport. We consider a single mode with $(m,n) = (2,3)$. Figure 3 shows the Poincare plots of the magnetic field in this case for perturbation amplitudes $\epsilon = 1 \times 10^{-4}$, $\epsilon = 3.95 \times 10^{-4}$, and $\epsilon = 9 \times 10^{-4}$. The initial temperature distribution for the transport calculation consisted of a linear profile of the form

$$T_0(\psi) = 1 - 2R^2\psi. \tag{33}$$

Figure 3 shows cuts along $\theta_1 = 2.14$ and $\theta_2 = 2.96$ of the computed asymptotic, steady state temperature distribution. As expected, plateaus in the temperature profile are observed at the location of the resonant islands. Most importantly, the separatrix reconnection characteristic of reversed shear configurations leads to nontrivial bifurcations in the radial temperature profiles. In particular, at the reconnection threshold the temperature plateaus collide and, after reconnection, a reverse gradient in the asymptotic temperature profile, due to the meandering curves wrapping around the islands, is observed.

B. Weakly chaotic fields and destruction of shearless temperature transport barrier

When two modes are added the system ceases to be integrable and chaotic field lines appear in the Poincare plots. In the calculations we use two modes with the same amplitude ϵ, and $(m,n) = \{(2,3),(7,10)\}$. As shown in Fig. 4, for $\epsilon = 10^{-4}$, a banded chaos regime (i.e., well-defined flux surfaces flanked by chaotic bands) is observed in the Poincare plot. For the larger amplitude $\epsilon = 3.38 \times 10^{-4}$, the chaotic bands grow, but a resilient shearless integrable flux surface is observed. For $\epsilon = 5 \times 10^{-4}$ the shearless flux surface breaks and the magnetic field exhibits widespread chaos. The steady state temperature profiles in Fig. 4 reflect the chaotic structure of the field lines. In particular, for $\epsilon = 10^{-4}$, the banded chaos in the magnetic field gives rise to two temperature plateaus,

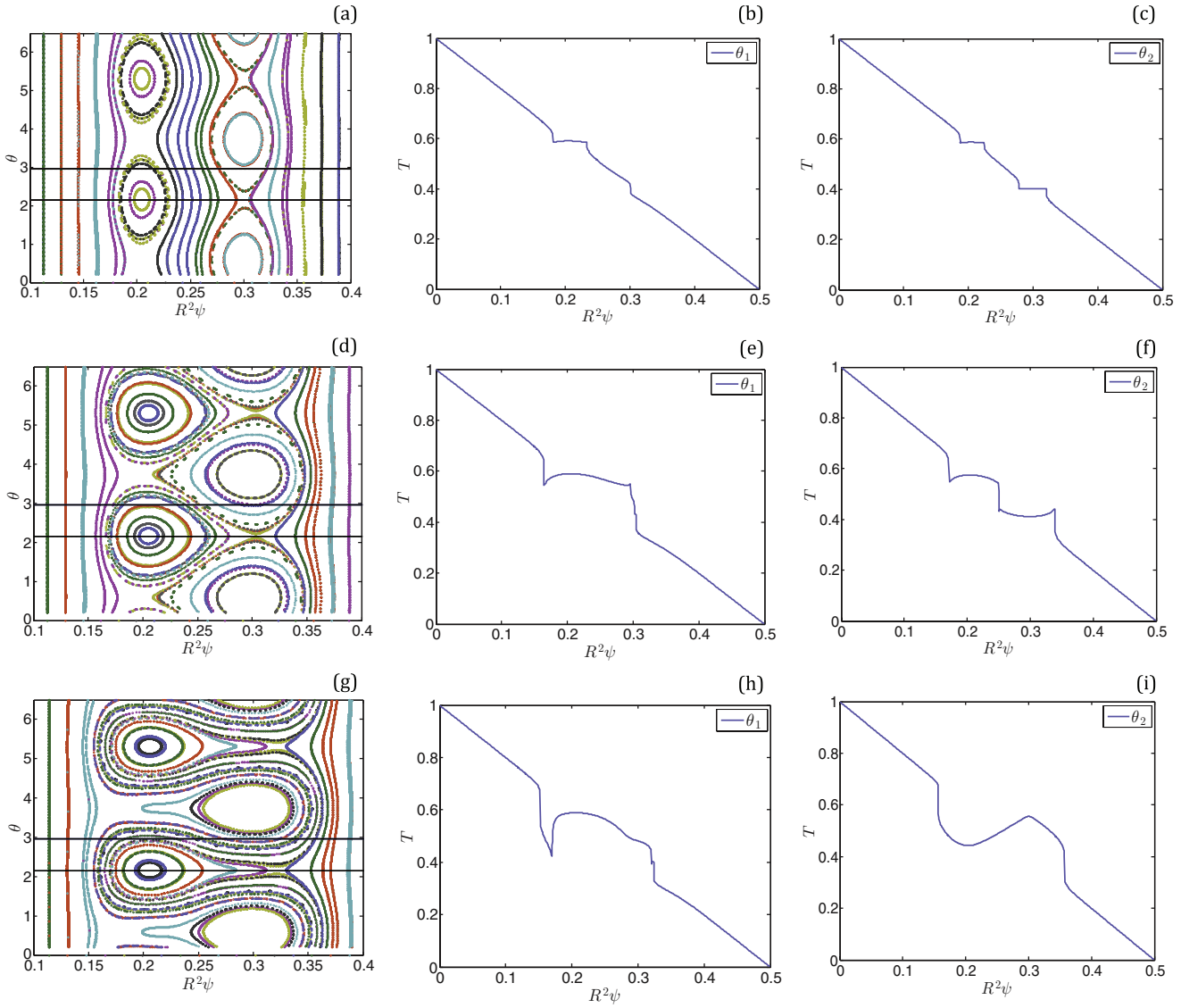

FIG. 3. (Color online) Bifurcations in the steady state radial temperature profiles due to separatrix reconnection in the magnetic field as function of the perturbation amplitude ϵ and initial temperature distribution in Eq. (33). The left column shows the Poincare plots for single-mode perturbations with $(m,n) = (2,3)$ and (a) $\epsilon = 1 \times 10^{-4}$, (d) $\epsilon = 3.95 \times 10^{-4}$, and (g) $\epsilon = 9 \times 10^{-4}$. The middle (right) column shows the corresponding $\theta_1 = 2.14$ ($\theta_2 = 2.96$) cuts of the asymptotic steady state temperature profiles.

resulting from the strong mixing in the chaotic regions, separated by a temperature gradient maintained by the flux surfaces in the reversed shear region. Near the threshold for the destruction of the shearless flux surface, i.e., for $\epsilon = 3.38 \times 10^{-4}$, the two chaotic mixing plateaus expand and approach each other but a very sharp temperature gradient separating the two regions is observed. For the larger amplitude $\epsilon = 5 \times 10^{-4}$, the destruction of the shearless flux surfaces gives rise to the merging of the two temperature plateaus and to the creation to an extended, albeit noisy, plateau in the temperature profile.

C. Shearless Cantori and multiscale temperature relaxation

At the threshold of the transition to chaos, magnetic field lines trace Cantor-like fractal sets in the Poincare section. This is a generic property of chaotic Hamiltonian systems [17,19]. Following the dynamical systems terminology, we refer to critical magnetic surfaces at the reversed shear region as "shearless Cantori." Cantori are partial barriers in the sense that although they do not fully confine the magnetic field, transport across them can be anomalously slow. The goal of this subsection is to study the role of these structures on the effective radial transport of heat.

Figure 5 shows the Poincare plot and the corresponding asymptotic $\chi_\parallel t = 10^6$ temperature distribution in the presence of the 17 modes

$$(m,n) = \{(2,3),(7,10),(4,5),(9,10),(13,15),\\ (12,13),(3,4),(11,12),(14,15),(7,8),(8,9),\\ (11,13),(6,7),(11,10),(14,17),(5,6),(9,11)\}, \quad (34)$$

with amplitude $\epsilon = 3.75 \times 10^{-4}$. Although for this amplitude most of the field lines are chaotic, a robust shearless transport

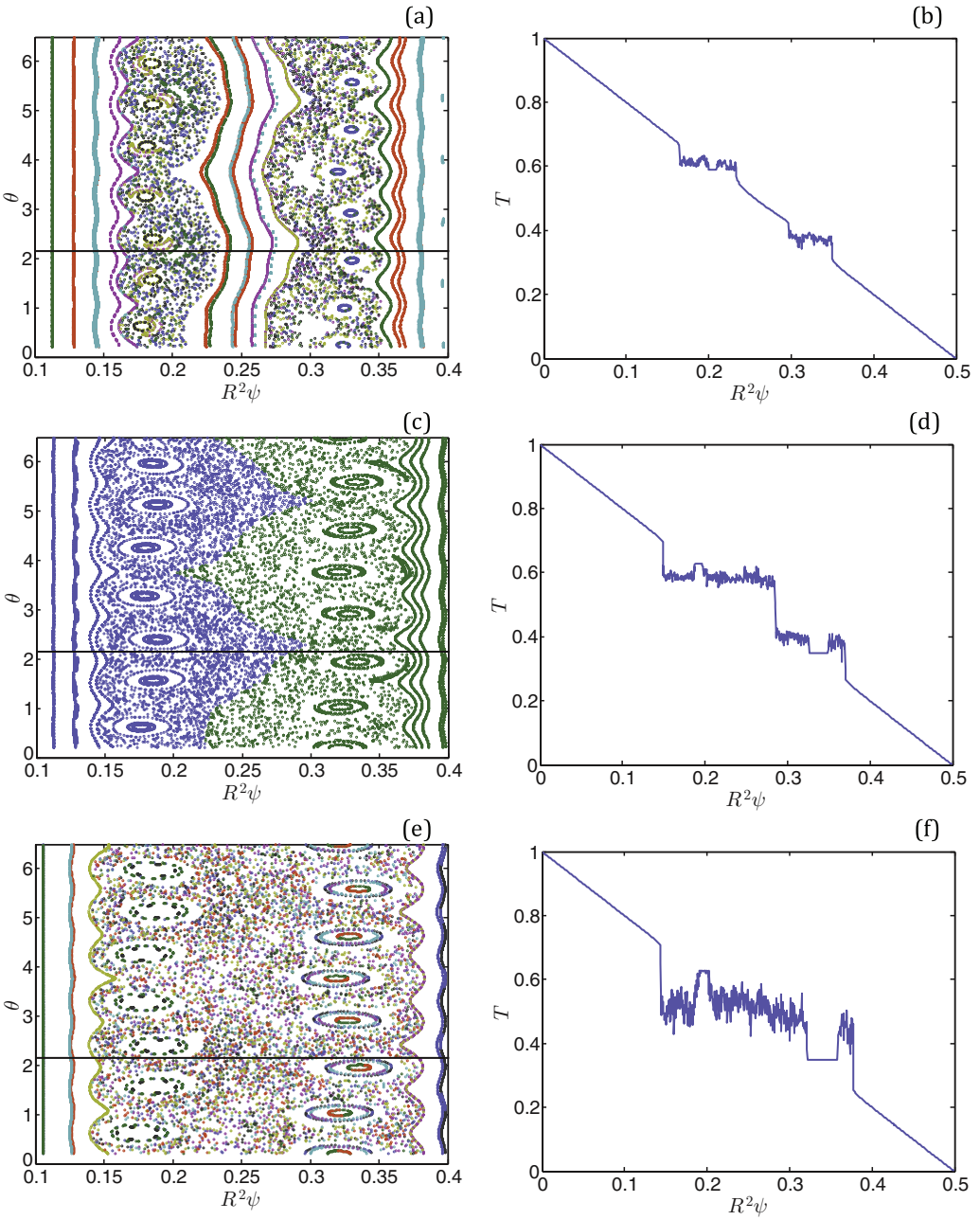

FIG. 4. (Color online) Heat transport in weakly chaotic and fully chaotic magnetic fields with two modes with $(m,n) = \{(2,3),(7,10)\}$, and initial temperature distribution in Eq. (33). The left column shows the Poincare plots, and the right column shows the corresponding steady state radial temperature profiles. (a) and (b) Correspond to the banded chaos regime with perturbation amplitude $\epsilon = 10^{-4}$. (c) and (d) Correspond to the threshold of the destruction of the shearless curve with $\epsilon = 3.38 \times 10^{-4}$. (e) and (f) Correspond to the global chaos regime with $\epsilon = 5 \times 10^{-4}$.

barrier is still observed in the Poincare plot along with a sharp temperature gradient in the reversed shear region. In this case, the initial condition T_0 consisted of the superposition of a positive temperature pulse on the left and a negative temperature pulse on the right of the $q' = 0$ line. Because of the shearless barrier, there is no mixing of the positive and negative temperature distributions. To study the role of shearless Cantori, the previous calculation was repeated with a slightly increased amplitude $\epsilon = 4.1 \times 10^{-4}$. The resulting Poincare section is shown in Fig. 6 for a single field line with 500 crossings (left panel) and for 600 crossings (right panel). The key point to observe is that, although there are no transport barriers for this amplitude, the migration of the chaotic field lines across the reversed shear region is retarded due to the existence of partial transport barriers. This phenomenon is related to the anomalous escape rate of magnetic field orbits discussed in Ref. [20].

Given the nature of the field lines depicted in Fig. 6, we expect heat flux across the reversed shear region to be anomalously slow. To study this, we consider the evolution

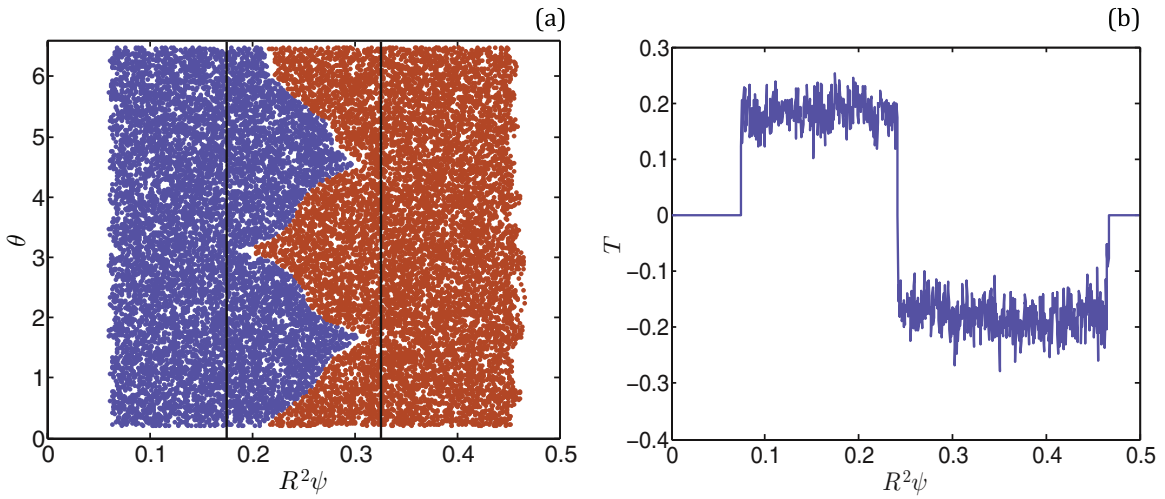

FIG. 5. (Color online) Robustness of shearless magnetic flux surface and radial heat transport barrier in the presence of the modes in Eq. (34) with perturbation amplitude $\epsilon = 3.75 \times 10^{-4}$. (a) The Poincare plot for two magnetic field lines: one started at the left of the reversed shear region, and the other started at the right of this region. Despite the widespread chaotic behavior exhibited by the two field lines, a resilient shearless flux surface precludes the crossing between these two regions. As a result, the radial temperature profile at $\theta = 2.14$, shown in (b), exhibits a sharp gradient. The two vertical lines on (a) indicate the radial region outside which a flat temperature distribution is observed.

of an initial condition with a linear profile of the form in Eq. (33), and compute the evolution of the radial temperature profile averaged in z and θ, $\langle T\rangle(\psi)$, and the corresponding radial flux

$$\langle \mathbf{q}\cdot\hat{e}_\psi\rangle = -\frac{1}{\sqrt{2\psi}}\frac{d}{dt}\int_0^\psi \langle T\rangle d\psi', \tag{35}$$

obtained directly from the continuity equation. The evaluation of the flux in Eq. (35) is numerically challenging because the radial profile $\langle T\rangle(\psi)$ can be noisy in chaotic regions (e.g., Figs. 4 and 5). For short time scales (relative to the slow evolution of the mixing) this can give rise to a small signal to noise ratio in the computation of the time derivative. For example, the change of the radial temperature in the time window $\chi_\parallel t \in (10^7, 10^7 + 10^5)$ is practically undistinguishable from the noise level. A numerically accessible and robust way to circumvent this problem is to approximate the flux $\langle \mathbf{q}\cdot\hat{e}_\psi\rangle$ at time $\chi_\parallel t$ by its average $q_{\rm avg}$ over the interval $[\chi_\parallel t - \Delta t, \chi_\parallel t + \Delta t]$,

$$\begin{aligned} q_{\rm avg}(\chi_\parallel t, \Delta t) &= \frac{1}{2\Delta t}\int_{\chi_\parallel t-\Delta t}^{\chi_\parallel t+\Delta t} \langle \mathbf{q}\cdot\hat{e}_\psi\rangle(s) ds \\ &= -\frac{1}{2\Delta t}\frac{1}{\sqrt{2\psi}}\int_0^\psi \langle T\rangle(\chi_\parallel t + \Delta t) \\ &\quad - \langle T\rangle(\chi_\parallel t - \Delta t) d\psi'. \end{aligned} \tag{36}$$

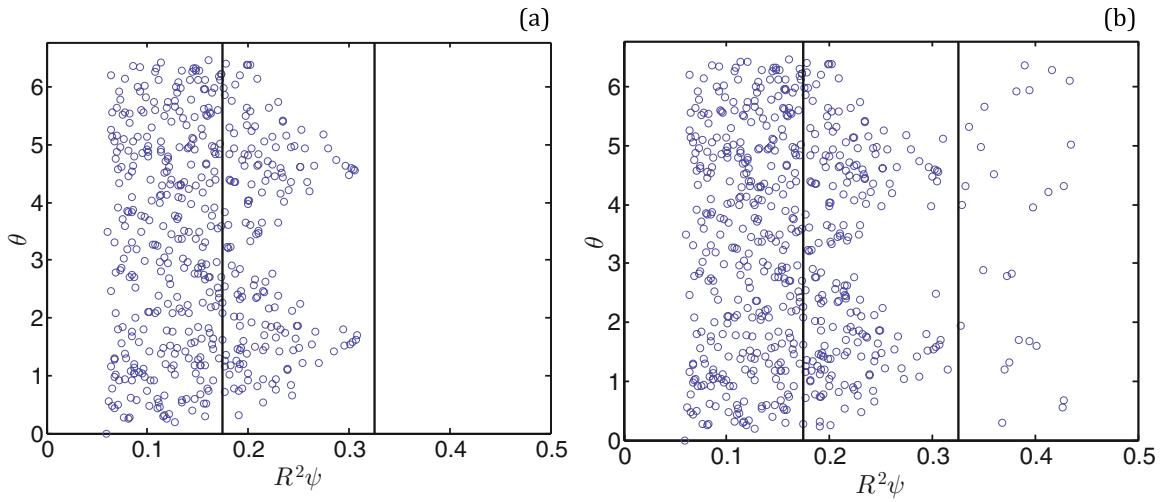

FIG. 6. (Color online) Slow leak of magnetic field lines across the reversed shear region in the presence of the modes in Eq. (34) with perturbation amplitude $\epsilon = 4.1 \times 10^{-4}$. (a) The Poincare plot of a single magnetic field that remains confined to the left of the shearless region by Cantori partial barriers for up to 500 crossings. As (b) shows, for 600 crossings the magnetic field eventually crosses to the right side. The vertical lines are the same as those shown in Fig. 5.

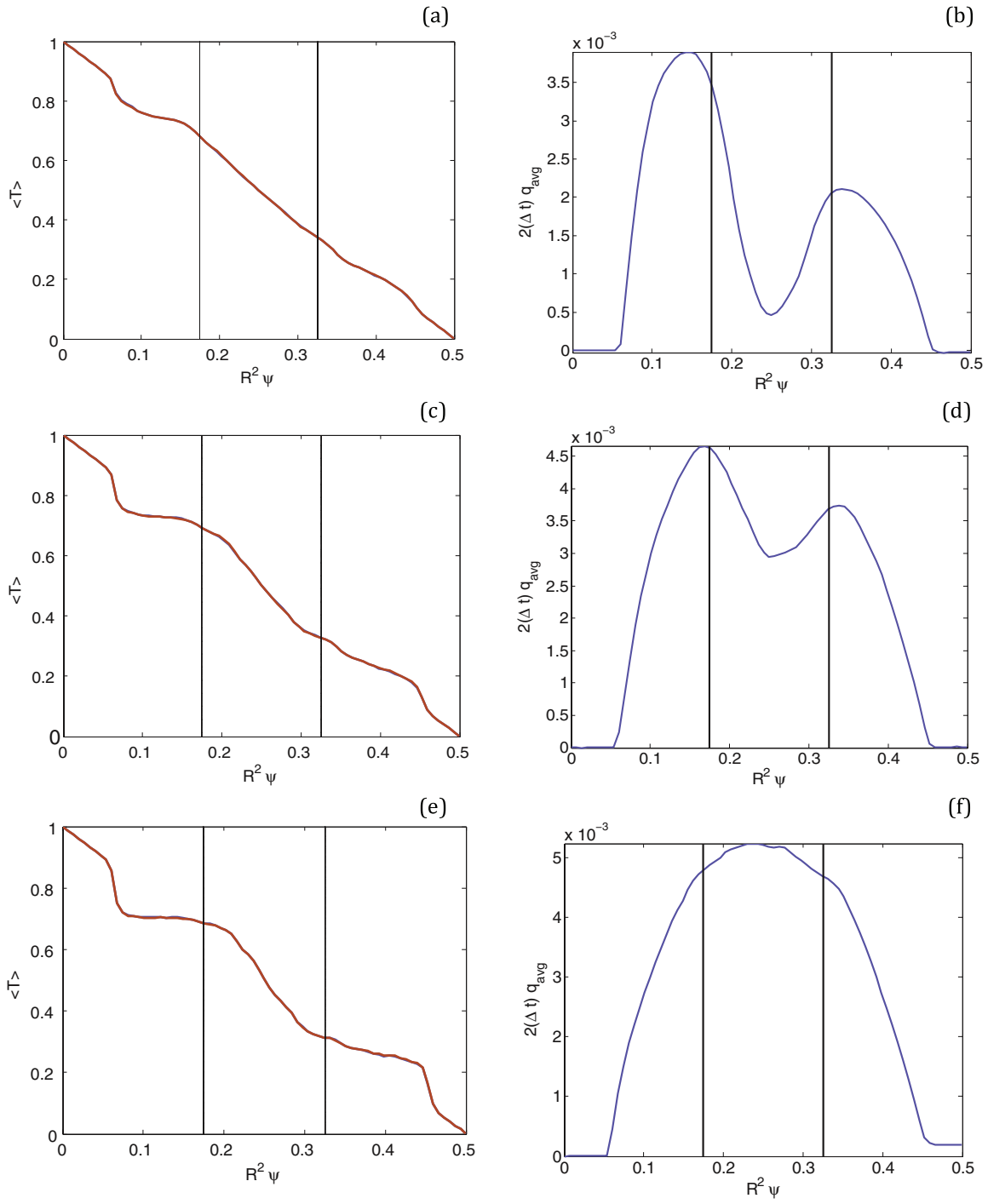

FIG. 7. (Color online) Short time behavior of anomalous temperature relaxation in the presence of shearless Cantori for the magnetic field in Fig. 6. The right column shows the flux averaged over $\chi_\parallel t \in [95,105]$ in (b), [950,1050] in (d), and [9500,10500] in (f). The left column shows the corresponding temperature profiles at the endpoints of these intervals, e.g., $T(\chi_\parallel t = 95,x)$ and $T(\chi_\parallel t = 105,x)$ in (a) and so on. Note that due to the small change in $\chi_\parallel t$, these profiles are practically undistinguishable. The vertical lines are the same as those shown in Fig. 5.

The selection of the time interval Δt is a subtle issue as it has to be large enough to increase the signal to noise ratio and small enough so that the change in time of the profile is captured accurately. For short time scales, the temperature profiles $\langle T \rangle$ tend to be smooth, but for large time scales they tend to be noisy. Although this noise can be significantly reduced using finer grids in (z,θ), there seems to be an irreducible noise level due to the nonergodicity of temperature mixing in chaotic regions.

For relatively small time scales, e.g., $\chi_\parallel t = 10^k, k = 2,3,4$, we have observed that $\Delta t/\chi_\parallel t = 0.1$ gives a good signal-to-noise ratio in the computation of the flux. Figure 7 shows

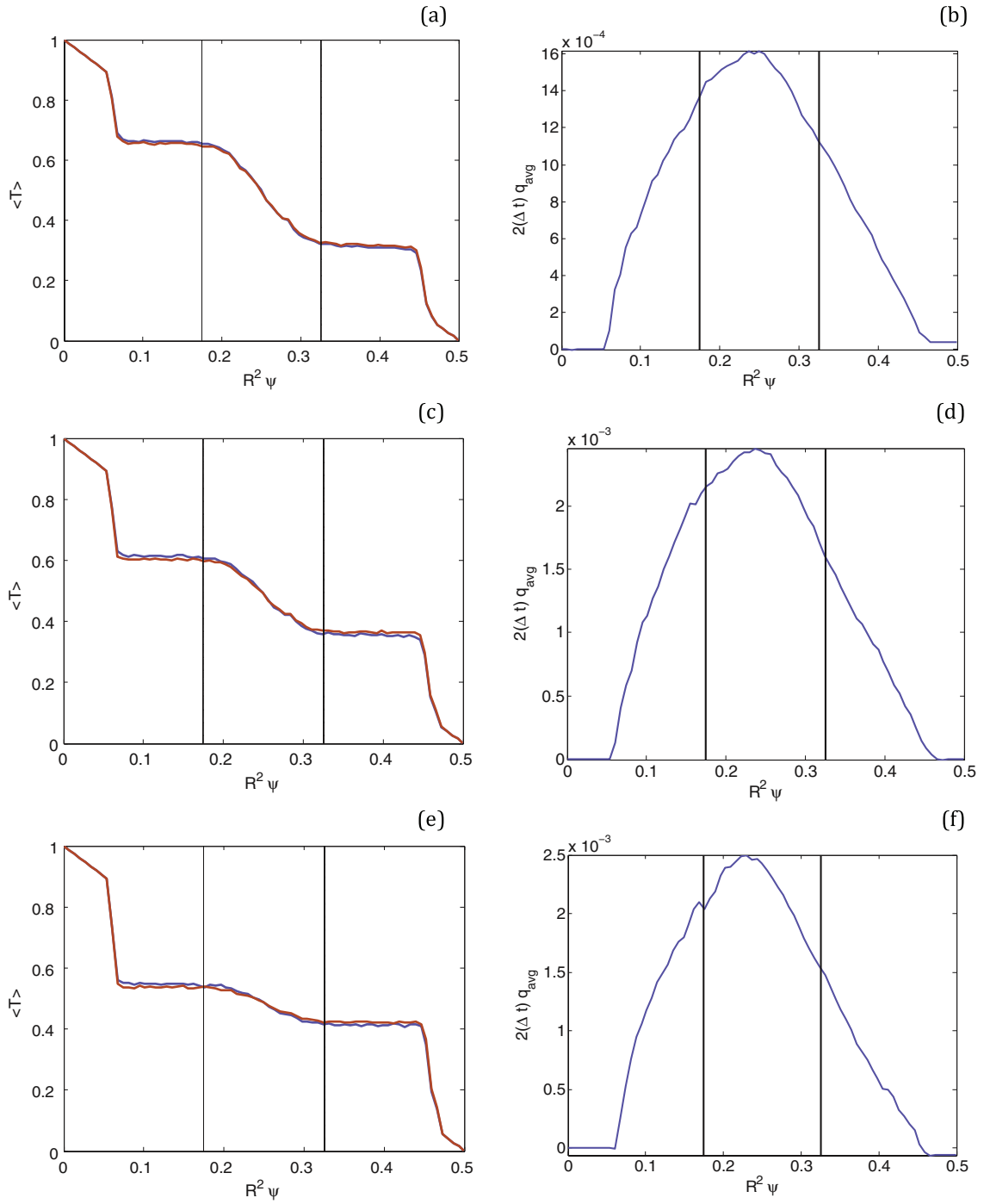

FIG. 8. (Color online) Long time behavior of anomalous temperature relaxation in the presence of shearless Cantori for the magnetic field in Fig. 6. The right column shows the flux averaged over $\chi_\parallel t \in [4\times10^5, 6\times10^5]$ in (b), $[4\times10^6, 6\times10^6]$ in (d), and $[4\times10^7, 6\times10^7]$ in (f). The left column shows the corresponding temperature profiles at the endpoints of these intervals, e.g., $T(\chi_\parallel t = 4\times10^5, x)$ and $T(\chi_\parallel t = 6\times10^5, x)$ in (a) and so on. Note that due to the relatively small change in $\chi_\parallel t$, these profiles are very similar. The vertical lines are the same as those shown in Fig. 5.

the numerically computed flux in this case along with the corresponding radial profiles. It is observed that the averaged flux in the time interval [95,105] is peaked in the chaotic regions on the left and right of the reversed shear region, and has a minimum in the middle where the shearless Cantori are present. For later times, it is observed that, once the temperature begins to flatten in the left and right chaotic bands, the radial flux bifurcates and exhibits a maximum in the reversed shear region.

To account for the increase in the noise level of the profiles at later times, we use $\Delta t/\chi_\parallel t = 0.5$ to compute $q_{\rm avg}(\chi_\parallel t, \Delta t)$ for $\chi_\parallel t = 5\times10^k, k = 5,6,7$. The results in this case are reported in Fig. 8. It is observed that, in this time scale, the temperature profiles are flat in the chaotic bands and the transport is

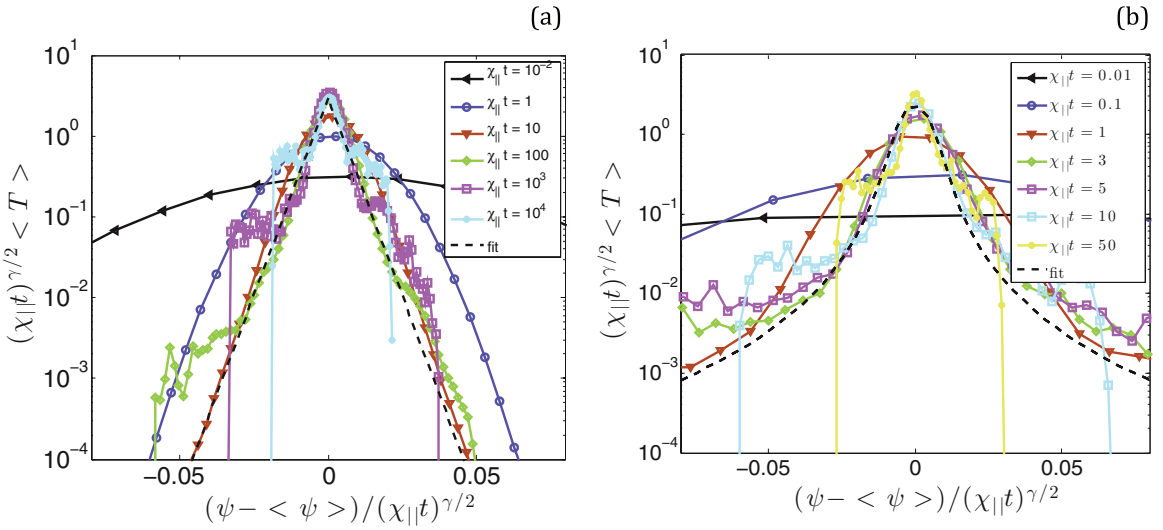

FIG. 9. (Color online) Spatio-temporal dynamics of average radial temperature profiles plotted in self-similar variables. The magnetic field corresponds to the one in Fig. 6, and the initial temperature distribution is in Eq. (37). In (a), which corresponds to the local parallel flux closure in Eq. (5), $\gamma = 0.5$. In (b), which corresponds to the nonlocal parallel flux closure in Eq. (9), with $\alpha = 1$, $\gamma = 1$.

dominated by an anomalously slow erosion of the temperature gradient in the reversed shear region.

D. Self-similarity and strong nonlocal radial temperature transport

To study the spatio-temporal evolution of the temperature profile in the reversed shear region in more detail, we consider the transport of a localized initial temperature profile of the form

$$T_0 = \exp\left[-\frac{R^4(\psi - \psi_0)^2}{\sigma^2}\right], \tag{37}$$

with $R^2\psi_0 = 0.25$ and $\sigma = 0.02$. Of particular interest is to compare the evolution of $\langle T\rangle$ in the reversed shear case with the results reported in Refs. [1,2] that assumed a monotonic q profile. Also of interest is to explore the departures from the Fourier-Fick's diffusion paradigm due to nonlocal transport processes.

In Refs. [1,2] it was observed that $\langle T\rangle$ exhibits self-similar evolution of the form

$$\langle T\rangle(\psi,t) = (\chi_{\|}t)^{-\gamma/2}L(\eta), \tag{38}$$

with scaling variable $\eta = (\psi - \bar{\psi})/(\chi_{\|}t)^{\gamma/2}$, and scaling exponent γ. Subdiffusive scaling ($\gamma = 1/2$) was found for the parallel diffusion closure in Eq. (5), and diffusive scaling ($\gamma = 1$) was found for the parallel fractional closure in Eq. (9) with $\alpha = 1$. As Fig. 9 shows, in the reversed shear magnetic field case studied in the present paper, similar scaling exponents are found, although the level of self-similarity is weaker as judged by the poorer level of self-similar collapse of the profiles.

In the intermediate asymptotic regime, where self-similarity is present, it is interesting to explore the shape of the self-similarity function $L(\eta)$. These functions are shown Fig. 10 for the case of diffusive and $\alpha = 1$ fractional diffusive parallel closures. For comparison, we have also included the corresponding results for the monotonic q-profile case reported in Refs. [1,2]. As discussed in Refs. [1,2], in the diffusive closure case, L is well fitted by an stretched exponential function, whereas in the $\alpha = 1$ fractional diffusive parallel closure case, L exhibits algebraic decay. However, as Fig. 10 shows, in the reversed shear case the behavior of the scaling functions is different. In particular, clear scaling is only observed in the reversed shear region where L is well fitted by an exponential function.

Although as Fig. 9 shows, the scaling in the reversed shear case is approximately self-similar, there are some differences with the monotonic q case. One way to explore these differences is to study the scaling of the fractional moment

$$\sigma_{1/2} = \overline{(\psi - \bar{\psi})}^{1/2}, \tag{39}$$

where $\bar{f} = \int f\langle T\rangle d\psi / \int \langle T\rangle d\psi$, that puts more weight on the peak of the temperature distribution which is centered in the reversed shear region. Figure 11 compares the time evolution of the temperature maximum $T_{\max}$ and $\sigma_{1/2}$ for the monotonic and nonmonotonic q-profile cases. A clear delay in the decay of $T_{\max}$ and in the growth of $\sigma_{1/2}$ is observed. This delay is a manifestation of the Cantori that, as discussed before, slow down the transport process across the revered shear region. As the algebraic fits in dashed lines indicate, the self-similar evolution of $\langle T\rangle$ starts around $\sim\chi_{\|}t = 100$ for the nonmonotonic q profile versus the monotonic q profile that starts around $\sim\chi_{\|}t = 10$. The fact that the self-similar regime begins at a later time is expected since the Cantori slow down the relaxation process, especially when the heat is initially localized near the shearless region as is the case in these simulations.

To further compare the nonmonotonic and monotonic q cases, we compute the delay τ in the temperature evolution defined by the condition

$$f_t(\tau) = T^{nm}_{\max}(\chi_{\|}t + \tau) - T^{m}_{\max}(\chi_{\|}t) = 0, \tag{40}$$

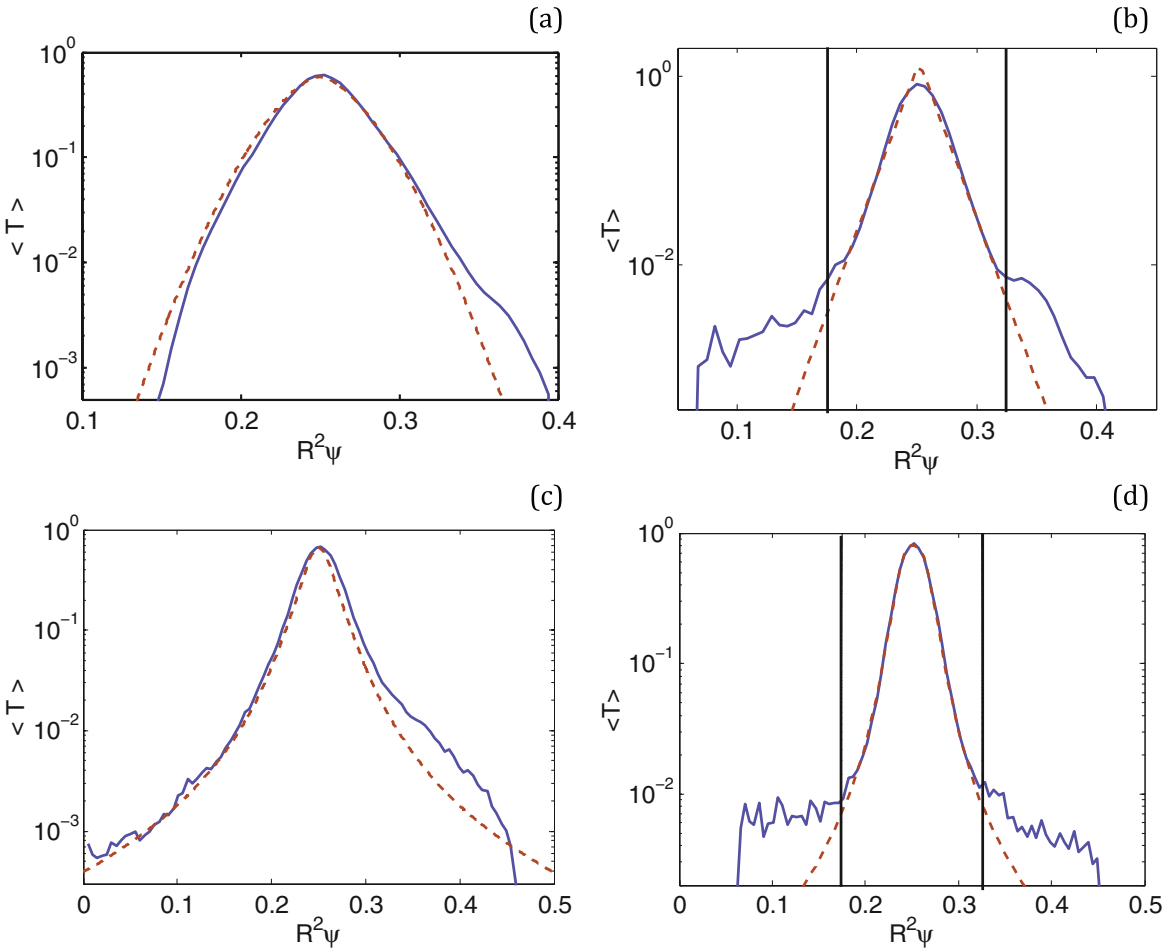

FIG. 10. (Color online) Comparison between the numerically computed averaged radial temperature profiles (solid blue lines) and corresponding fits (dashed red lines). The left column corresponds to the magnetic field configuration with monotonic q profile studied in Refs. [1,2]. The column on the right corresponds to the reversed shear magnetic field case. (a) and (b) Correspond to the diffusive parallel flux closure in Eq. (5), and (c) and (d) correspond to the nonlocal parallel flux closure in Eq. (9) with $\alpha = 1$. The vertical lines are the same as those shown in Fig. 5. In (b), $\chi_\parallel t = 200$, and in (d), $\chi_\parallel t = 8$.

where $T^m_{\max}$ ($T^{nm}_{\max}$) denotes the temperature maximum in the monotonic (nonmonotonic) q-profile case. To compute τ, we used Newton's method to solve Eq. (40). The result, shown in Fig. 11, indicates that the delay scales approximately linearly with t. A similar analysis can be applied to the $1/2$ moment, which as Fig. 11 shows, also exhibits a delay τ defined by the condition

$$\sigma^{nm}_{1/2}(\chi_\parallel t + \tau) - \sigma^{m}_{1/2}(\chi_\parallel t) = 0, \tag{41}$$

which scales approximately linearly with t.

To conclude this section we study the relation between the radial flux in Eq. (35) and the radial temperature gradient

$$\langle \nabla T \cdot \hat{e}_\psi \rangle = \frac{1}{\sqrt{2\psi}} \frac{\partial \langle T \rangle}{\partial \psi}. \tag{42}$$

Of particular interest is to test the applicability of the Fourier-Fick prescription, according to which these two quantities exhibit a linear relationship of the form

$$\langle \mathbf{q} \cdot \hat{e}_\psi \rangle = -\chi \langle \nabla T \cdot \hat{e}_\psi \rangle + V \langle T \rangle, \tag{43}$$

where χ is the effective diffusivity and V is an effective drift velocity, know in plasma physics as a "pinch." As discussed in Refs. [1,2], one way to study this problem is to plot the numerically computed flux and the gradient, along with the flux-gradient parametric curves

$$\mathcal{C} : \psi \to [-\langle \nabla T \cdot \hat{e}_\psi \rangle(\psi), \langle \mathbf{q} \cdot \hat{e}_\psi \rangle(\psi)]. \tag{44}$$

These plots are shown in Fig. 12 for the case of parallel diffusive closures and $\alpha = 1$ parallel fractional diffusion closures. The most striking feature observed is the presence of a finite flux in regions where the gradient vanishes, something that is also observed in Figs. 7 and 8. The only way to make the results in Fig. 12 consistent with Eq. (43) is by assuming the existence of a nonzero, spatially dependent pinch velocity, i.e., $V(\psi) \neq 0$. However, the existence of such an asymmetric pinch velocity is inconsistent with Fig. 8. This is because according to Fig. 8, the steady state $\partial_t \langle T \rangle = 0$ solution in $R^2\psi \in (0.05, 4.5)$ is $\langle T \rangle =$ constant, which implies $V \langle T \rangle = 0$, i.e., $V = 0$. Having ruled out the existence of a pinch velocity, the loops observed in the flux-gradient plots in Fig. 12 provide further evidence of the inapplicability of Fourier-Fick prescription unless an ad hoc spatial dependence of χ is assumed. Although such an spatial dependence might be

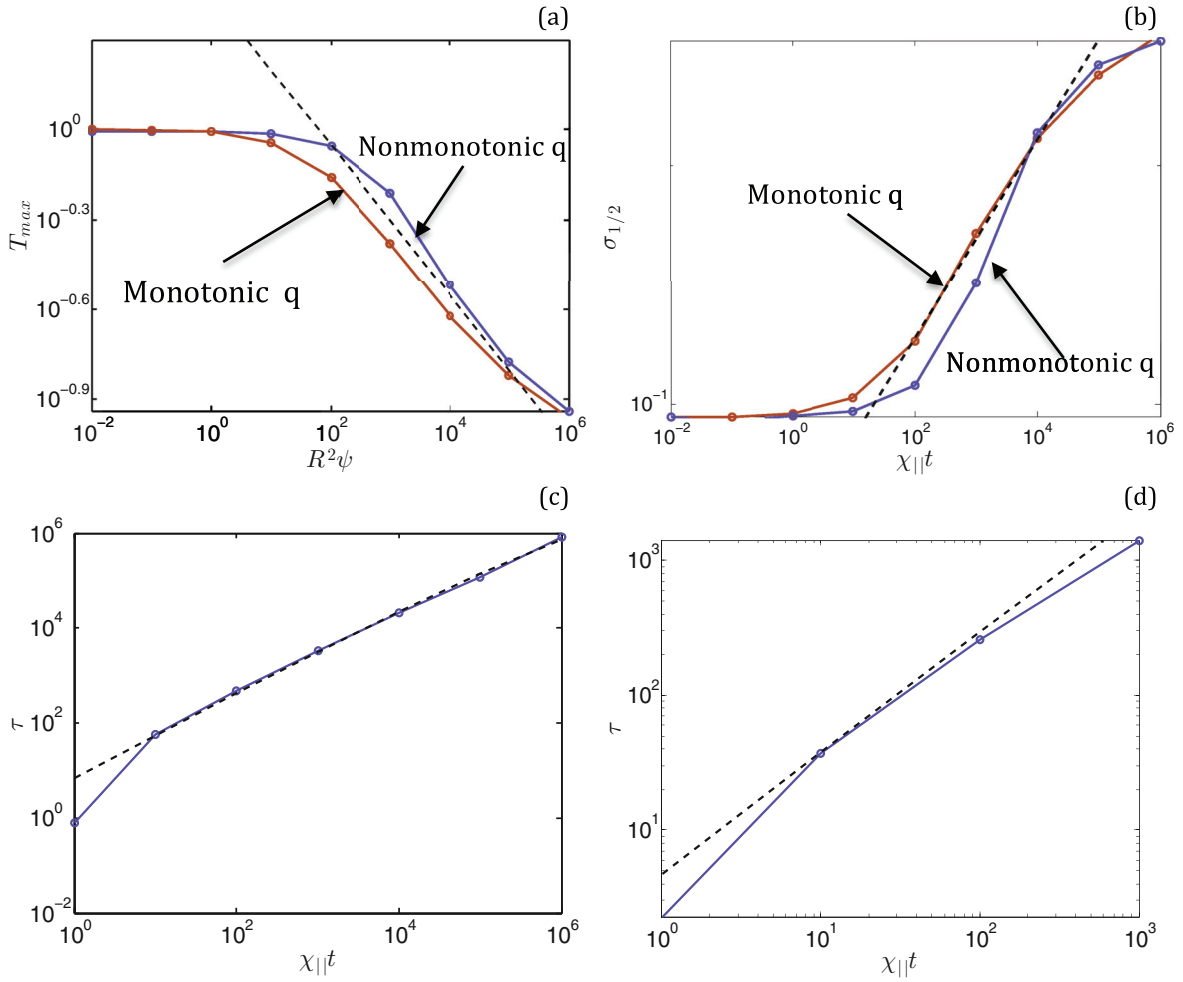

FIG. 11. (Color online) Temperature decay $T_{\max}$ in (a), and growth of the fractional moment $\sigma_{1/2}$ in (b), for monotonic and nonmonotonic q profiles, corresponding to the simulation in Fig. 9. (c) and (d) The delay time τ of $T_{\max}$ and $\sigma_{1/2}$, respectively.

conceivable, the strongest argument against the Fourier-Fick prescription is the existence of a finite flux in the presence of zero gradient.

V. SUMMARY AND CONCLUSIONS

We applied a Lagrangian-Green's (LG) function method to solve the anisotropic heat transport equation in reversed shear magnetic configurations characterized by nonmonotonic q profiles. From the dynamical systems perspective, these type of magnetic fields correspond to nontwist (degenerate) Hamiltonians known to exhibit robust transport KAM (Kolmogorov-Arnold-Moser) barriers. As a result, reversed shear magnetic field configurations typically have barriers to chaotic magnetic field line transport in the vicinity of the extrema of the q profile, i.e., shearless regions of the magnetic field. This key property makes these configurations particularly attractive to confinement, and an important problem in controlled nuclear fusion research is to understand the role of magnetic chaos suppression in shearless regions on heat transport.

Motivated by the extreme anisotropic encounter in fusion plasmas, we focused on pure parallel transport ($\chi_\perp = 0$). A particularly challenging aspect of this problem is that near-collisionless plasmas typically require the use of nonlocal closures for which the parallel heat flux depends on the global properties of the temperature distribution on the whole field line, and not just the local gradient. To model this we used, in addition to the standard local parallel diffusion equation, a parallel fractional diffusion equation.

Our main goal was to study the implications to heat transport of two key aspects of reversed shear magnetic configurations: separartrix reconnection and robust shearless flux surfaces. Separatrix reconnection is a generic property of nontwist Hamiltonian systems leading to bifurcations in the topology of the magnetic field lines in the reversed shear region. By solving the anisotropic transport equation for different parameters, we studied how the changes in the magnetic field topology lead to bifurcations in the equilibrium temperature distribution.

Like in the monotonic q case, the addition of several resonant perturbations to reversed shear equilibria typically leads to magnetic-field-line chaos through island overlap. However, there are several key differences. In particular, in reversed shear configurations, for perturbations of moderate amplitudes, magnetic chaos is restricted to bands flanking the shearless region and, before the central shearless magnetic

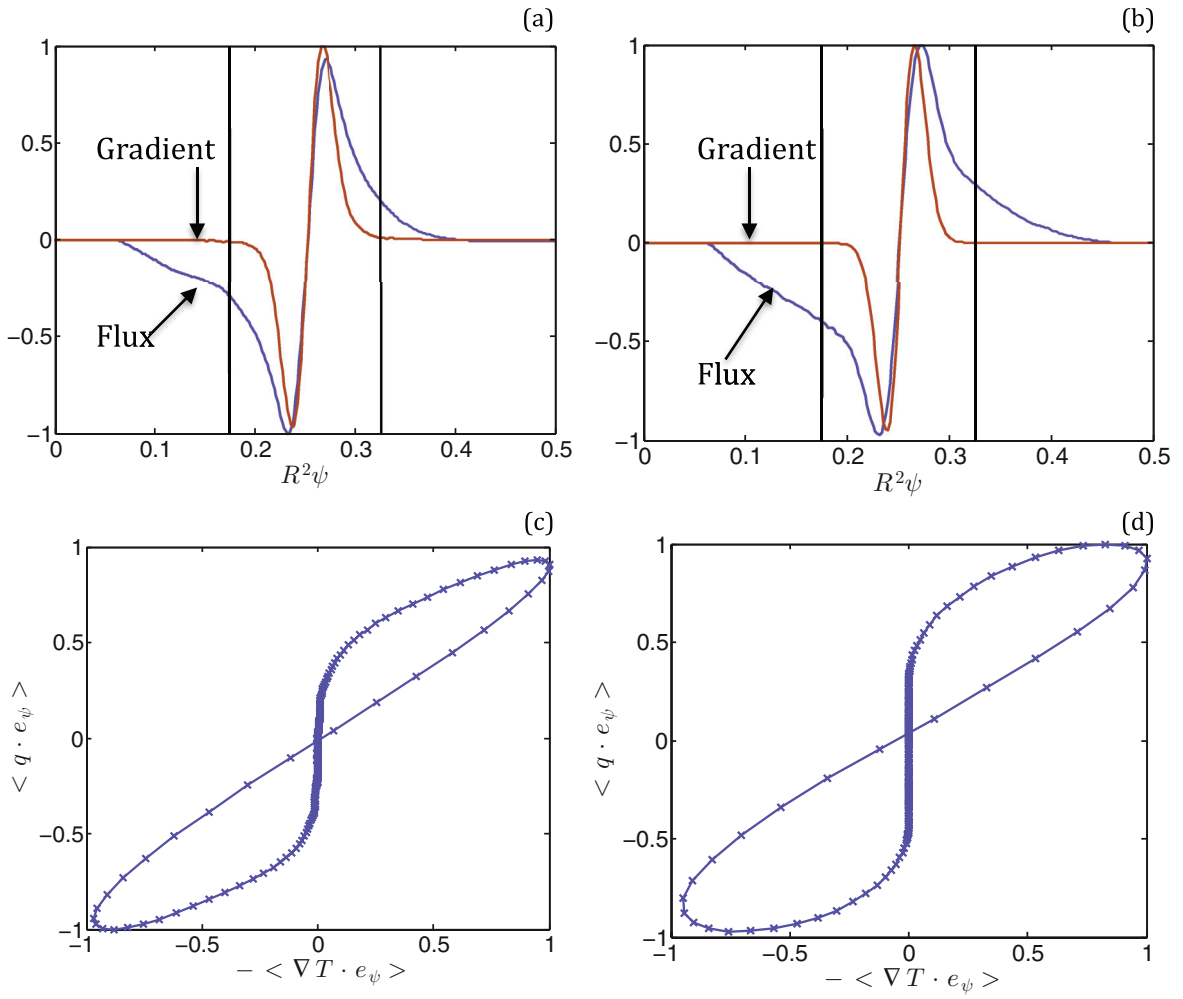

FIG. 12. (Color online) Nonlocal effective radial transport corresponding to the simulation in Fig. 9. The left column corresponds to the local diffusive parallel closure in Eq. (5), at $\chi_\parallel t = 200$ and the right column to the nonlocal free streaming closure in Eq. (9) with $\alpha = 1$ at $\chi_\parallel t = 8$. (a) and (b) The profiles of the flux and temperature gradient. (c) and (d) The corresponding flux-gradient parametric curves.

surface breaks, most of the magnetic field is already chaotic. Here we have shown that, as a result, the temperature exhibits intense mixing that locally flattens the radial profile in the chaotic bands, and, at the same time, it exhibits a very sharp radial gradient in the shearless region.

At the threshold of the transition to chaos, the Poincare sections of critical magnetic field lines trace Cantor-like fractal sets known as Cantori. Cantori are partial barriers in the sense that they do not fully confine the magnetic field but the transport across them can be anomalously slow. To explore the role of shearless Cantori (i.e., critical magnetic surfaces located at minimum of the q profile) on the radial transport of temperature, we studied the relaxation of a linear temperature distribution in a reversed shear chaotic magnetic field. We observed that the relaxation is a multiscale process involving widely different time scales. The first stage consists of the relatively fast ($\chi_\parallel t \sim 10^2$) flattening of the radial profile in the chaotic bands flanking the reversed shear region. During this stage, the flux exhibits two peaks centered in the chaotic bands, and a minimum in the reversed shear region. This minimum results from the anomalously slow leakage across this region due to the presence of shearless Cantori. For practical proposes, on this time scale, there is an effective temperature transport barrier despite the fact that there are no magnetic flux surfaces. However, once the temperature has fully mixed in the chaotic bands, the flux develops a maximum in the shearless region on the long time scale $\chi_\parallel t \sim 10^5$. During this second stage, heat starts to flow across the shearless, albeit at a comparatively low rate. The final fully mixed state in which the temperature is flat across the whole domain occurs occurs on a long time scale of the order $\chi_\parallel t \sim 10^7$.

To further explore the role of shearless Cantori, we considered the transport of a narrow temperature pulse centered at the minimum of the q profile, for diffusive and fractional diffusive parallel closures. In all cases, we observed that the radial temperature profiles exhibit weak self-similarity, with non-Gaussian scaling functions indicating that effective radial transport at this scale cannot be modeled as a diffusive process with a constant diffusivity. Related to this, we provided evidence of nonlocal effective radial transport in reversed shear chaotic fields. In particular, the numerical results showed regions where the flux is finite but the gradient is zero. The

possibility of invoking the existence of a pinch velocity to describe this anomalous behavior of the flux is not fully consistent with the data.

ACKNOWLEDGMENTS

This work was sponsored by the Office of Fusion Energy Sciences of the US Department of Energy at Oak Ridge National Laboratory, managed by UT-Battelle, LLC, for the US Department of Energy under Contract No. DE-AC05-00OR22725. The authors thank Luis Chacón for providing the code implementing the LG method. D.B. acknowledges the hospitality of the Oak Ridge National Laboratory and the School of Mathematics at The Georgia Institute of Technology during the elaboration of this work.

[1] D. del-Castillo-Negrete and L. Chacon, Phys. Rev. Lett. **106**, 195004 (2011).
[2] D. del-Castillo-Negrete and L. Chacon, Phys. Plasmas **19**, 056112 (2012).
[3] R. Lorenzini *et al.*, Nat. Phys. **5**, 570 (2009).
[4] R. Lorenzini *et al.*, Nucl. Fusion **52**, 062004 (2012).
[5] V. I. Arnold, *Mathematical Methods of Classical Mechanics* (Springer, New York, 1974).
[6] D. del-Castillo-Negrete, J. M. Greene, and P. J. Morrison, Physica D **91**, 1 (1996).
[7] D. del-Castillo-Negrete, J. M. Greene, and P. J. Morrison, Physica D **100**, 311 (1997).
[8] D. del-Castillo-Negrete and P. J. Morrison, Bull. Am. Phys. Soc. Ser. II **37**, 1543 (1992).
[9] R. Balescu, Phys. Rev. E **58**, 3781 (1998).
[10] M.-C. Firpo and D. Constantinescu, Phys. Plasmas **18**, 032506 (2011).
[11] C. G. L. Martins, R. Egydio de Carvalho, I. L. Caldas, and M. Roberto, Physica A **390**, 957 (2011).
[12] E. D. Held, J. D. Callen, C. C. Hegna, and C. R. Sovinec, Phys. Plasmas **8**, 1171 (2001).
[13] D. del-Castillo-Negrete, Phys. Plasmas **13**, 082308 (2006).
[14] J. E. Howard and S. M. Hohs, Phys. Rev. A **29**, 418 (1984).
[15] J. P. van der Weele and T. P. Valkering, Physica A **169**, 42 (1990).
[16] A. Wurm, A. Apte, K. Fuchss, and P. J. Morrison, Chaos **15**, 023108 (2005).
[17] R. S. Mackay *et al.*, Physica D **13**, 55 (1984).
[18] L. Chacon, D. del-Castillo-Negrete, and C. D. Hauck, J. Comput. Phys. (unpublished).
[19] S. R. Hudson, Phys. Rev. E. **74**, 056203 (2006).
[20] T. Kroetz *et al.*, Phys. Plasmas **15**, 092310 (2008).